

Chaotic Response of an Airfoil due to Aeroelastic Coupling and Dynamic Stall

V. Laxman* and C. Venkatesan†

Indian Institute of Technology, Kanpur 208 016, India

DOI: 10.2514/1.24587

Flight-test data of helicopters indicate that vibratory levels in the fuselage exhibit a wide spectrum of frequencies, including a few below the rotor revolutions per minute. It is well known that helicopter blades operate in a complex aerodynamic environment, involving time-varying heave, pitch, and pulsating oncoming flow. During operation, some sections of the rotor blade undergo dynamic stall once in a revolution. This paper attempts to understand the reason for the existence of several frequencies in the response of the fuselage and the possible cause for this observed phenomenon by analyzing the effects of dynamic stall and aeroelastic couplings on the response of 2-D airfoil. The ONERA dynamic stall model developed by Petot is modified by incorporating a higher-order rational approximation of Theodorsen's lift deficiency function. This improved model is shown to provide a better correlation with experimental stall data. The response characteristics of a 2-D airfoil undergoing pitching and plunging motion in a pulsating oncoming flow, simulating the response of a cross section of a helicopter rotor blade in forward flight are analyzed. This study shows significant difference in the response characteristics of the airfoil for unsteady (dynamic stall model) and quasi-steady aerodynamic models. It is observed that the nonlinear aerodynamics (dynamic stall effects) in association with aeroelastic couplings above a certain level lead to a bounded chaotic motion of the airfoil.

Nomenclature

b	= semichord
C_D	= unsteady drag coefficient
C_{d_L}	= linear static drag coefficient extrapolated to the stall region
C_M	= unsteady moment coefficient
C_{m_L}	= linear static moment coefficient extrapolated to the stall region
C_Z	= unsteady lift coefficient
C_{z_L}	= linear static lift coefficient extrapolated to the stall region
$C(k)$	= Theodorsen's lift deficiency function
I_ϕ	= moment of inertia about elastic axis
h	= heaving motion of an airfoil
k	= reduced frequency, $\omega b/V$
K_h	= linear spring constant in heaving motion
K_ϕ	= linear torsional spring constant in pitching motion
L	= lift on airfoil
M	= moment on airfoil about elastic axis, nose up is positive
M_∞	= Mach number
m	= mass of airfoil
\tilde{S}	= area of airfoil
S_ϕ	= static moment about elastic axis
t	= time
V	= oncoming velocity
\tilde{V}	= amplitude of time-varying part of oncoming velocity
V_0	= mean value of oncoming velocity
Γ_{d_2}	= aerodynamic state in stalled region in drag equation
Γ_{m_2}	= aerodynamic state in stalled region in moment equation
Γ_1	= aerodynamic state in unstalled region in lift equation
Γ_2	= aerodynamic state in stalled region in lift equation

Presented as Paper 1866 at the 47 AIAA/ASME/ASCE/AHS/ASC SDM Conference, Newport, RI, 1–4 May 2006; received 12 April 2006; revision received 23 August 2006; accepted for publication 4 October 2006. Copyright © 2006 by V. Laxman and C. Venkatesan. Published by the American Institute of Aeronautics and Astronautics, Inc., with permission. Copies of this paper may be made for personal or internal use, on condition that the copier pay the \$10.00 per-copy fee to the Copyright Clearance Center, Inc., 222 Rosewood Drive, Danvers, MA 01923; include the code \$10.00 in correspondence with the CCC.

*Graduate student, Department of Aerospace Engineering. Student Member AIAA.

†Professor, Department of Aerospace Engineering. Senior Member AIAA.

θ	= pitch angle, deg
$\tilde{\theta}$	= amplitude of time-varying pitch angle
θ_d	= static stall angle
θ_{eff}	= effective pitch angle
θ_0	= mean value of pitch angle
ρ	= density of air
τ	= nondimensional time, Vt/b
ϕ	= elastic twist
Ω	= input excitation frequency
ω	= excitation frequency
ω_h	= natural frequency of the heaving motion
ω_ϕ	= natural frequency of the pitching motion

I. Introduction

THE field of rotary-wing elasticity has been a very active area of research during the last four decades [1]. There are still several unresolved issues relating to blade loads and fuselage response in forward flight [2]. One such problem is the existence of frequencies below the rotor revolutions per minute, in the vibratory signature of the fuselage, as observed in flight-test data of several helicopters [3]. In general, nonlinear effects are often cited as possible reasons for any observed difference between theory and experiment [4]. The major sources of nonlinearity in rotary wing aeroelasticity are due to 1) geometric nonlinearity associated with moderate deformation of the rotor blade, and 2) aerodynamic nonlinearity due to dynamic stall. This study is an attempt to understand the possible cause for the observed phenomenon in flight-test data, by the formulation and solution of a nonlinear aeroelastic response problem, involving dynamic stall effects.

Rotor blade aerodynamic modeling is highly complex due to time-varying pitch, heave, pulsating oncoming flow, dynamic stall, and wake effect. During forward flight, some sections of the rotor blade undergo dynamic stall once in a revolution. Modeling of instantaneous sectional lift, drag, and moment as functions of pitching, plunging motion of the blade, variation in oncoming velocity and inflow velocity is of paramount importance in evaluating rotor aerodynamic loads. Therefore theoretical prediction of fuselage response is largely dependent on the ability to accurately model the rotor blade unsteady aerodynamic loads, in and out of stall.

Dynamic stall is a strong nonlinear unsteady aerodynamic effect associated with flow separation and reattachment. Several experimental [5–9] and theoretical [10–21] studies are available in

the open literature on dynamic stall of a 2-D airfoil undergoing pitching, plunging motion and time-varying oncoming flow. Most of the experimental studies on dynamic stall phenomenon have focused on airfoils oscillating only in pitching motion [5,6]. Steady and unsteady aerodynamic characteristics of several airfoil sections were investigated by McCroskey et al. [6]. The parameters that were varied under dynamic stall conditions were Mach number, reduced frequency, mean angle, and amplitude of the oscillation. The principal ranges of reduced frequency k , mean angle θ_0 , and amplitude of oscillation $\tilde{\theta}$ were $0.01 \leq k \leq 0.20$, $\theta_0 = 10$ and 15 deg, and $\tilde{\theta} = 2, 5$, and 10 deg, respectively; and the effects of these parameters were studied primarily at $M_\infty = 0.30$. A comparative study on the effect of pitching and plunging motions of an oscillating airfoil has been reported by Carta [7] and Ericsson and Reding [8]. The experimental data show that for low angle of attack (about $\theta = 2$ deg), pitching and plunging motions have similar effect on the lift and moment characteristics; however, for high angles of attack (about $\theta = 8$ deg), considerable differences were observed. The combined effect of time-varying oncoming velocity and pitching motion on the aerodynamic behavior of a NACA 0012 airfoil was investigated by Favier et al. [9]. In this study, a cam mechanism was designed to generate variation in oncoming velocity and pitch angle in the form $V = V_0 + \tilde{V} \cos \omega t$ and $\theta = \theta_0 + \tilde{\theta} \sin(\omega t + \Phi)$. Two values of θ_0 ($\theta_0 = 6$ and 12 deg) are chosen to analyze the airfoil characteristics in attached and separated flow regimes. It may be noted that there is no experimental study available in the open literature on the combined effects of pitching, plunging, and oncoming flow velocity variations on the aerodynamic characteristics of a 2-D airfoil.

Theoretical models that attempt to predict the effects of dynamic stall range from relatively simple semiempirical models to sophisticated computational fluid dynamics (CFD) methods. One of the earliest semiempirical models for dynamic stall was developed by Beddoes [10]. In this model, aerodynamic lift and moment on airfoil in attached flow regime is obtained from Duhamel superposition integral using the Wagner indicial response function. Corrections are applied to the Wagner function to account for the effects of compressibility. Gangwani [11] developed a synthesized airfoil method for the prediction of dynamic stall. To model the airloads in attached flow, a Mach-scaled Wagner function is used in the Duhamel superposition integral. In the separated flow regime, a set of algebraic equations with several empirical coefficients is used to represent the unsteady aerodynamic coefficients of the airfoil. Leishman and Beddoes [12] have developed a model capable of representing unsteady lift, pitching moment, and drag characteristics of an oscillating airfoil in pitching motion using the Wagner function and flow separation point on the suction side of the airfoil, identified by Kirchoff flow idealization. This model was later extended to include heaving motion [13] and pulsating motion [14]. ONERA (EDLin) model developed by Petot [15] describes the unsteady airfoil behavior in both attached flow and separated flow of a pitching airfoil using a set of nonlinear differential equations. Peters [16] modified Petot's model [15] by including the effects of heaving and pulsating oncoming flow in the lift expression and referred to it as "unified lift model." Based on the observations of Peters [16], Petot [17] proposed an extended dynamic stall model including the effects of pitching, plunging, and oncoming flow velocity variations. The coefficients of the differential equations of this extended model are determined by parameter identification using experimental measurements on oscillating airfoils. ONERA(BH) model developed by Troung [18], uses a Vander Pol Duffing type nonlinear equation to represent the separated flow conditions; however, in the attached flow region, it retains the equation developed by Petot [17]. In [19], a detailed description of the state of art in dynamic stall modeling has been presented. Recently CFD methods [20,21] are applied to predict dynamic stall in airfoils. Because semiempirical stall models can be easily integrated to aeroelastic analysis, ONERA and Leishman-Beddoes dynamic stall models are used in the literature for aeroelastic applications [22–27]. Depailler and Friedmann [28] combined rational function approximation and ONERA stall model

to represent unsteady load in attached flow and separated flow regimes, respectively, for the analysis of vibration in helicopters. In [29,30], the authors have studied the effects of structural nonlinearity and ONERA dynamic stall model on the response of a rotor blade. They have shown that the necessary condition for the onset of chaotic response is that the system must be near flutter boundary. When the flutter speed is low, the chaotic motion is determined by the structural nonlinearity and for high flutter speeds, chaotic motion is dominated by nonlinearity due to aerodynamic stall.

In this paper, ONERA(EDLin) dynamic stall model has been analyzed in relation to Theodorsen's and Greenberg's unsteady aerodynamic theories. Based on this analysis, an improved dynamic stall model is proposed. It is shown that the improved model provides better correlation with experimental dynamic stall data. Subsequently, a nonlinear aeroelastic problem of a 2-D airfoil is studied to bring out the effects of dynamic stall and aeroelastic couplings on the response characteristics of the airfoil.

II. Extended ONERA (EDLin) Dynamic Stall Model

The extended ONERA(EDLin) stall model [17] provides time variation of lift, moment, and drag on an oscillating airfoil. The stall model assumes that the lift, moment, and drag are acting at the quarter-chord point. The unsteady lift acting normal to the resultant velocity is given as

$$L = \frac{1}{2} \rho \tilde{S} [sb \dot{W}_0 + \tilde{k} b \dot{W}_1 + V \Gamma_1 + V \Gamma_2] \quad (1)$$

$$\begin{aligned} \dot{\Gamma}_1 + \lambda \left(\frac{V}{b} \right) \Gamma_1 &= \lambda \left(\frac{V}{b} \right) \frac{\partial C_{zL}}{\partial \theta} W_0 + \lambda \sigma \left(\frac{V}{b} \right) W_1 \\ &+ \left(\tilde{\alpha} \frac{\partial C_{zL}}{\partial \theta} + d \right) \dot{W}_0 + \tilde{\alpha} \sigma \dot{W}_1 \end{aligned} \quad (2)$$

$$\begin{aligned} \ddot{\Gamma}_2 + a \left(\frac{V}{b} \right) \dot{\Gamma}_2 + r \left(\frac{V}{b} \right)^2 \Gamma_2 &= - \left[r \left(\frac{V}{b} \right)^2 V \Delta C_z|_{W_0/V} \right. \\ &\left. + E \left(\frac{V}{b} \right) \dot{W}_0 \right] \end{aligned} \quad (3)$$

The unsteady moment on the airfoil is given as

$$\begin{aligned} M &= \frac{1}{2} \rho \tilde{S} 2b [V^2 C_{mL}|_{W_0/V} + (\tilde{\sigma}_m + d_m) b \dot{W}_0 + \sigma_m V W_1 \\ &+ s_m b \dot{W}_1 + V \Gamma_{m2}] \end{aligned} \quad (4)$$

$$\begin{aligned} \ddot{\Gamma}_{m2} + a_m \left(\frac{V}{b} \right) \dot{\Gamma}_{m2} + r_m \left(\frac{V}{b} \right)^2 \Gamma_{m2} &= - \left[r_m \left(\frac{V}{b} \right)^2 V \Delta C_m|_{W_0/V} \right. \\ &\left. + E_m \left(\frac{V}{b} \right) \dot{W}_0 \right] \end{aligned} \quad (5)$$

The unsteady drag acting along the resultant velocity is given as

$$D = \frac{1}{2} \rho \tilde{S} [V^2 C_{dL}|_{W_0/V} + \sigma_d b \dot{W}_0 + V \Gamma_{d2}] \quad (6)$$

$$\begin{aligned} \ddot{\Gamma}_{d2} + a_d \left(\frac{V}{b} \right) \dot{\Gamma}_{d2} + r_d \left(\frac{V}{b} \right)^2 \Gamma_{d2} &= - \left[r_d \left(\frac{V}{b} \right)^2 V \Delta C_d|_{W_0/V} \right. \\ &\left. + E_d \left(\frac{V}{b} \right) \dot{W}_0 \right] \end{aligned} \quad (7)$$

where W_0 and W_1 are defined as $W_0 = V(\dot{h}/V + \theta)$ and $W_1 = b\dot{\theta}$. \dot{h} represents the heaving velocity at elastic axis. $\Delta C_z|_{W_0/V}$, $\Delta C_m|_{W_0/V}$, and $\Delta C_d|_{W_0/V}$ are the difference between the linear static

aerodynamic coefficient extrapolated to the stalled region to actual static aerodynamic coefficient of lift, moment, and drag, respectively, measured at an effective angle of attack $W_0/V = \dot{h}/V + \theta$. $C_{m_L}|_{W_0/V}$ and $C_{d_L}|_{W_0/V}$ are the static moment and drag coefficients in linear regime measured at an effective angle of attack $W_0/V = \dot{h}/V + \theta$. It is to be noted that the effective angle of attack is to be specified in degrees.

The various coefficients [17][‡] of the lift model [Eqs. (1–3)] are given as

$$\begin{aligned} s &= \{\pi + 5\pi[(1 - M_\infty^2)^{0.285} - 1]\} \frac{\pi}{180} \\ \tilde{k} &= \left(\frac{\pi}{2} + 1.96\pi[\sqrt{(1 - M_\infty^2)} - 1]\right) \frac{\pi}{180} \quad \lambda = 0.17 - 0.13M_\infty \\ \sigma &= \left(\frac{2\pi}{\sqrt{(1 - M_\infty^2)}}\right) \frac{\pi}{180} \quad \tilde{\alpha} = 0.53 + 0.25(\sqrt{1 - M_\infty^2} - 1) \\ d &= d_1 |\Delta C_z| \quad a = a_0 + a_1 \Delta C_z^2 \quad \sqrt{r} = r_0 + r_1 \Delta C_z^2 \\ E &= E_1 \Delta C_z^2 \end{aligned}$$

The various coefficients of the moment model [Eqs. (4) and (5)] are given as

$$\begin{aligned} \tilde{\sigma}_m &= -\frac{\pi}{4}[1 + 1.4M_\infty^2] \frac{\pi}{180} \\ d_m &= \sigma_{1m} |\Delta C_z| \quad (\sigma_{1m} \text{ varies between 0 and 0.15} \\ &\quad \text{depending on the airfoil}) \\ s_m &= -\frac{3\pi}{16}\{-1.26 - 1.53 \arctan[15(M_\infty - 0.7)]\} \frac{\pi}{180} \\ \sigma_m &= \sigma_{0m} + \sigma_{1m} |\Delta C_z| \\ \sigma_{0m} &= \left(\frac{3\pi}{16}\{-1.26 - 1.53 \arctan[15(M_\infty - 0.7)]\}\right. \\ &\quad \left.- \frac{\pi}{2}[1 + 1.4M_\infty^2]\right) \frac{\pi}{180} \\ a_m &= a_{m_0} + a_{m_1} \Delta C_z^2 \quad \sqrt{r_m} = r_{m_0} + r_{m_1} \Delta C_z^2 \\ E_m &= E_{m_1} \Delta C_z^2 \end{aligned}$$

The various coefficients of the drag model [Eqs. (6) and (7)] are given as

$$\begin{aligned} \sigma_d &= \sigma_{0d} \theta + \sigma_{1d} |\Delta C_z| \quad (\sigma_{1d} \text{ varies between 0 and} \\ &\quad -0.05 \text{ depending on the airfoil}) \\ \sigma_{0d} &= 0.003 \quad a_d = a_{d_0} + a_{d_1} \Delta C_z^2 \quad \sqrt{r_d} = r_{d_0} + r_{d_1} \Delta C_z^2 \\ E_d &= E_{d_1} \Delta C_z^2 \end{aligned}$$

The parameters $d_1, a_0, a_{m_0}, a_{d_0}, a_1, a_{m_1}, a_{d_1}, r_0, r_{m_0}, r_{d_0}, r_1, r_{m_1}, r_{d_1}, E_1, E_{m_1}$, and E_{d_1} have to be determined by parameter identification approach using experimental measurements on oscillating airfoils.

For an airfoil oscillating under unstalled conditions, Eq. (1) can be simplified by taking $\Gamma_2 = 0$ and $\Delta C_z = 0$ as

$$L = \frac{1}{2} \rho \tilde{S} [sb \dot{W}_0 + \tilde{k} b \dot{W}_1] + \frac{1}{2} \rho \tilde{S} [V \Gamma_1] \quad (8)$$

This expression for lift can be split into two parts as

$$L = L_{NC} + L_C \quad (9)$$

$$L_{NC} = \frac{1}{2} \rho \tilde{S} [sb \dot{W}_0 + \tilde{k} b \dot{W}_1] \quad (10)$$

$$L_C = \frac{1}{2} \rho \tilde{S} [V \Gamma_1] \quad (11)$$

Taking Laplace transform of Eq. (2) and substituting for Γ_1 in Eq. (11), the expression L_C can be written as

$$L_C = \frac{1}{2} \rho \tilde{S} V \left(\frac{[\tilde{\alpha} S(b/V) + \lambda]}{[S(b/V) + \lambda]} \left[\frac{\partial C_{z_L}}{\partial \theta} W_0 + \sigma W_1 \right] \right) \quad (12)$$

Assuming harmonic motion for the airfoil (i.e., setting Laplace variable $S = i\omega$), taking lift curve slope $\partial C_{z_L}/\partial \theta = 2\pi$, and substituting for W_0 and W_1 , the expressions for L_{NC} and L_C for low Mach number can be written as (note: the angle θ is changed from degrees to radians)

$$L_{NC} = \frac{1}{2} \rho \tilde{S} \pi [b(\ddot{h} + V\dot{\theta}) + \frac{1}{2} b^2 \ddot{\theta}] \quad (13)$$

$$L_C = \frac{1}{2} \rho \tilde{S} V 2\pi \left(\frac{[0.53(i\omega b/V) + 0.17]}{[i\omega b/V + 0.17]} [\dot{h} + V\theta + b\dot{\theta}] \right) \quad (14)$$

The expressions L_{NC} and L_C are, respectively, identical to the noncirculatory and circulatory parts of the unsteady lift obtained by Theodorsen [31], except for the lift deficiency function $C(k)$. In Eq. (14), the underlined term represents a first-order rational approximation to $C(k)$, which approximately satisfies the conditions at $k = 0$, $C(k) = 1$ and $k = \infty$, $C(k) \cong 0.5$. Higher-order rational functions have been shown to provide excellent correlation to lift deficiency function $C(k)$. A second-order approximation [32] to exact Theodorsen lift deficiency function is given as

$$C(k) \cong \frac{A_1(i\omega b/V)^2 + A_2(i\omega b/V) + A_3}{(i\omega b/V)^2 + B_2(i\omega b/V) + B_3} \quad (15)$$

where $A_1 = 0.50$, $A_2 = 0.393$, $A_3 = 0.0439425$, $B_2 = 0.5515$, and $B_3 = 0.0439075$. A comparison of first-order approximation and second-order approximation [32] with exact Theodorsen lift deficiency function [$C(k) = F(k) + iG(k)$] is shown in Fig. 1. It can be seen that second-order rational approximation shows better correlation with exact $C(k)$ than the first-order approximation. Replacing first-order approximation by the second-order rational approximation in Eq. (14) and applying Laplace inverse transform, the modified lift equations are obtained. They are given as

$$L = \frac{1}{2} \rho \tilde{S} [sb \dot{W}_0 + \tilde{k} b \dot{W}_1 + V \Gamma_1 + V \Gamma_2] \quad (16)$$

$$\begin{aligned} \ddot{\Gamma}_1 + B_2 \left(\frac{V}{b} \right) \dot{\Gamma}_1 + B_3 \left(\frac{V}{b} \right)^2 \Gamma_1 &= A_3 \left(\frac{V}{b} \right)^2 \frac{\partial C_{z_L}}{\partial \theta} W_0 \\ + A_3 \sigma \left(\frac{V}{b} \right)^2 W_1 + A_2 \left(\frac{V}{b} \right) \frac{\partial C_{z_L}}{\partial \theta} \dot{W}_0 + A_2 \left(\frac{V}{b} \right) \sigma \dot{W}_1 \\ + A_1 \frac{\partial C_{z_L}}{\partial \theta} \ddot{W}_0 + A_1 \sigma \ddot{W}_1 \end{aligned} \quad (17)$$

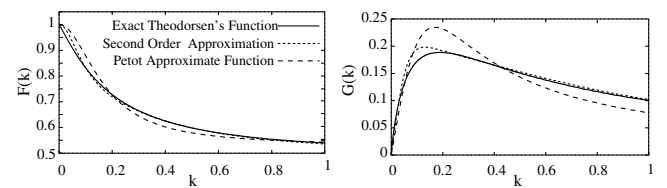


Fig. 1 Theodorsen's lift deficiency function.

[‡]D. Petot, private communication, 2005.

$$\ddot{\Gamma}_2 + a\left(\frac{V}{b}\right)\dot{\Gamma}_2 + r\left(\frac{V}{b}\right)^2\Gamma_2 = -\left[r\left(\frac{V}{b}\right)^2V\Delta C_z|_{W_0/V} + E\left(\frac{V}{b}\right)\dot{W}_0\right] \quad (18)$$

In the modified lift model, the aerodynamic state Γ_1 is given by a second-order differential equation [Eq. (17)], whereas original Petot model has a first-order differential equation [Eq. (2)]. The modified lift model will be shown to provide a better correlation with experimental stall data in both stalled and unstalled conditions. In this paper, the set of Eqs. (16–18) is referred to as “modified stall model” and the set of Eqs. (1–3) is denoted as Petot stall model. There is no change in the form of moment and drag equations, given by Eqs. (4–7), respectively.

In the unstalled region, Petot model lift can be shown to reduce to Greenberg’s theory. Replacing the first-order rational function by exact lift deficiency function $C(k)$ in Eq. (14), assuming $V = V_0 + \tilde{V}e^{i\omega_v t}$, $\theta = \theta_0 + \tilde{\theta}e^{i\omega_\theta t}$, $h = \tilde{h}e^{i\omega_h t}$, and substituting for W_0 and W_1 , the noncirculatory and circulatory lift expressions given in Eqs. (13) and (14) can be written as

$$L_{NC} = \frac{1}{2}\rho\tilde{S}\{[\pi b(\dot{V}\theta + V\dot{\theta} + \ddot{h}) + \frac{\pi}{2}b^2\ddot{\theta}]\} \quad (19)$$

$$L_C = \frac{1}{2}\rho\tilde{S}V(2\pi)C(k)[V_0\theta_0 + V_0\tilde{\theta}e^{i\omega_\theta t} + \theta_0\tilde{V}e^{i\omega_v t} + \tilde{V}\tilde{\theta}e^{i(\omega_\theta + \omega_v)t} + \dot{h} + b\dot{\theta}] \quad (20)$$

Replacing $C(k)$ using the frequency of the corresponding terms in Eq. (20), and combining with Eq. (19), the unsteady lift expression can be rewritten as

$$L = \frac{1}{2}\rho\tilde{S}\{[\pi b(\dot{V}\theta + V\dot{\theta} + \ddot{h}) + \frac{1}{2}\pi b^2\ddot{\theta}]\} + \frac{1}{2}\rho\tilde{S}V(2\pi)[V_0\theta_0 + (V_0\tilde{\theta}e^{i\omega_\theta t} + b\dot{\theta})C(k_\theta) + \theta_0\tilde{V}e^{i\omega_v t}C(k_v) + \tilde{V}\tilde{\theta}e^{i(\omega_\theta + \omega_v)t}C(k_{\theta+v}) + \dot{h}C(k_h)] \quad (21)$$

This lift expression is identical to the expression derived by Greenberg [33].

While performing an analysis of airfoil response, a comparative study of dynamic stall and quasi-steady aerodynamic models has been carried out to bring out effects of stall. Therefore, for the sake of completeness, the quasi-steady lift and moment (about quarter-chord point) expressions are given as follows. These expressions are obtained by setting $C(k) = 1$ in Greenberg’s unsteady lift and moment expressions[33].

$$L = \frac{1}{2}\rho\tilde{S}[\pi b(\dot{W}_0 + \frac{1}{2}\dot{W}_1) + V(2\pi W_0 + 2\pi W_1)] \quad (22)$$

$$M = \frac{1}{2}\rho\tilde{S}2b\left[-\frac{\pi}{4}b\dot{W}_0 - \frac{\pi}{4}VW_1 - \frac{3\pi}{16}b\dot{W}_1\right] \quad (23)$$

III. Results and Discussion

The results of this study are presented in two sections: 1) generation and validation of unsteady aerodynamic coefficients using the modified stall model, and 2) aeroelastic response of a 2-D airfoil under going pitching and plunging motion in pulsating oncoming flow.

Using the modified dynamic stall equations [Eqs. (16–18) for lift, Eqs. (4) and (5) for moment, and Eqs. (6) and (7) for drag], time variation of the aerodynamic coefficients are generated and compared with experimental data for three different cases, namely, 1) pure pitching motion of an airfoil, 2) pure plunging motion of an

airfoil, and 3) pitching motion of an airfoil in a pulsating oncoming flow. Results are also generated for combined pitching and plunging motion in a time-varying oncoming flow, simulating the cross-sectional motion of a helicopter rotor blade in operation.

A. Validation of Modified Stall Model

The aerodynamic coefficients are generated using the modified stall model for pitch, plunge, and pulsating oncoming flow. The static aerodynamic characteristics of a symmetric airfoil used in the present analysis are given in the Appendix. The various parameters used to generate the results are given as: for lift, $d = -0.04|\Delta C_z|$; $\sqrt{r} = 0.20 + 0.20\Delta C_z^2$; $a = 0.30 + 0.20\Delta C_z^2$; $E = -0.05\Delta C_z^2$; for moment, $d_m = 0$; $\sqrt{r_m} = 0.20 + 0.20\Delta C_z^2$; $a_m = 0.25 + 0.10\Delta C_z^2$; $E_m = 0.01\Delta C_z^2$; and for drag, $\sigma_d = 0.003\theta - 0.04|\Delta C_z|$; $\sqrt{r_d} = 0.20 + 0.20\Delta C_z^2$; $a_d = 0.25$; $E_d = -0.015\Delta C_z^2$. Blade semichord is taken as $b = 0.2$ m and the speed of sound used for calculating Mach number is assumed as 330 m/s.

The stall equations are converted into state-space form and fourth-order Runge–Kutta integration scheme has been used for evaluating the steady state response. The time step for integration is set at 0.00314 s and the initial conditions for aerodynamic states are assumed to be zero. In evaluating the response, the equations corresponding to stalled domain [Eq. (18) for lift, Eq. (5) for moment, and Eq. (7) for drag] have to be included in the solution procedure as soon as the effective pitch angle of the airfoil crosses the static stall angle during its motion.

1. Pitching Motion

First a comparison of the lift coefficient generated using modified dynamic stall model [Eqs. (16–18)] and Petot stall model [Eqs. (1–3)] is made with the experimental data of an airfoil undergoing only pitching motion. The airfoil is assumed to undergo a pitching motion $\theta = 15 + 10\cos(0.1\tau)$ deg. The Mach number is $M_\infty = 0.3$. The variation of lift coefficient for the two stall models are shown in Fig. 2 along with experimental data taken from [6]. The direction of variation of lift coefficient is indicated by arrows. It can be seen that the modified stall model proposed in this study provides a better correlation with experimental data, particularly in the reattachment zone represented by low values of C_Z ; however, it slightly underpredicts the maximum value of C_Z . It may be noted that the results presented in the following are generated using the modified stall model.

Keeping $M_\infty = 0.3$, the aerodynamic coefficients are generated for various reduced frequencies ($k = 0.03, 0.05$, and 0.1) of the pitching motion. The lift, moment, and drag coefficients generated from the modified stall model are shown in Fig. 3, along with the experimental data taken from [6]. The result shows that the modified stall provides a reasonably good correlation with experimental data. The correlation seems to be better for the case of lift than for moment and drag.

2. Pitching and Plunging Motion

For an unsymmetrical airfoil (NACA 23010), the time-varying lift and moment coefficients for pure pitching and pure plunging motion in attached flow are generated. The aerodynamic data used for this analysis are given in the Appendix. A comparison of the theoretical results with the experimental data (taken from [13]) is shown in Fig. 4a for pure pitching and Fig. 4b for pure plunging motion,

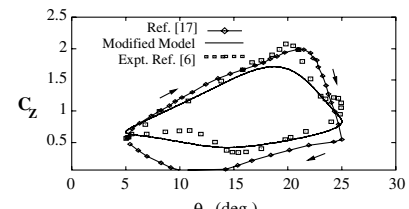


Fig. 2 Modified stall model compared with experimental data and Petot model: $\theta = 15 + 10\cos(0.1\tau)$ deg, $M_\infty = 0.3$.

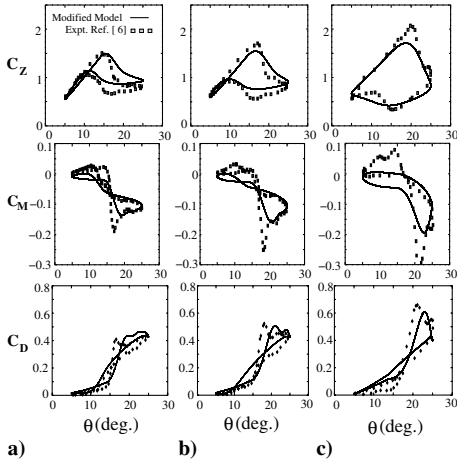


Fig. 3 Aerodynamic hysteresis loops generated for various reduced frequencies, $\theta = 15 + 10 \cos(k\tau)$ deg, $M_\infty = 0.3$: a) $k = 0.03$, b) $k = 0.05$, c) $k = 0.1$.

respectively. In the case of pure pitching motion, the pitch angle is varied as $\theta = 0.06 + 5.05 \sin(0.125\tau)$ deg. For the case of plunging motion, a mean pitch angle is set at 0.26 deg and the effective pitch angle is given by $\theta_{\text{eff}} = 0.26 + \bar{h}/V$, where $\bar{h} = \bar{h} \sin(0.125\tau)$. Mach number is taken as $M_\infty = 0.4$ and the reduced frequency is $k = 0.125$. The results indicate that the modified stall provides a reasonable/good correlation with experimental data for both lift and moment coefficients.

3. Pitching Motion in Pulsating Oncoming Flow

In [9], experimental studies have been carried out on a symmetric airfoil (NACA 0012) undergoing pitching motion in a pulsating oncoming flow. The oncoming flow velocity is given by $V = 6[1 + 0.356 \cos(0.314\tau)]$ m/s. The experiment was conducted for two pitch angle variations, one pertaining to the motion in the unstalled region, with $\theta = 6 + 6 \cos(0.314\tau + \Phi)$ deg and the other in the stalled region given by $\theta = 12 + 6 \cos(0.314\tau + \Phi)$ deg. Φ represents the phase angle between oncoming flow velocity and the pitching motion. Results are presented for the two cases of phase angles, i.e., $\Phi = 0$ and 180 deg. Figure 5 shows the comparison between experimental and theoretical stall data of unsteady lift coefficient. The results indicate that the modified stall model provides a better correlation with experimental data for both unstalled and stalled cases when $\Phi = 180$ deg (Figs. 5b and 5d). On the other hand, the correlation is not good for the case when $\Phi = 0$ deg (Figs. 5a and 5c). The reason for the poor correlation for this case may be attributed to the deficiency of the stall model in capturing the effect of the formation of a larger leading-edge bubble [9] as compared to the case of $\Phi = 180$ deg.

The variation of drag coefficient for pure pitching motion and pitching motion in pulsating oncoming flow is shown in Figs. 6a and

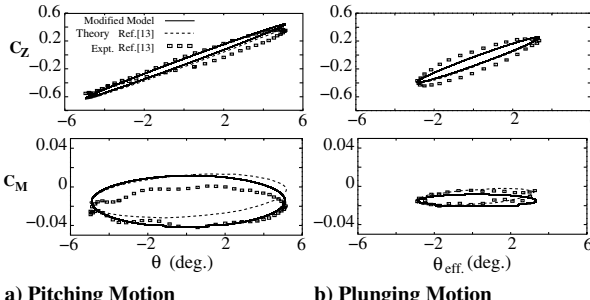


Fig. 4 Lift and moment coefficients generated for unsymmetrical airfoil for pitch and plunge motion. Pitching motion: $\theta = 0.06 + 5.05 \sin(0.125\tau)$ deg, $M_\infty = 0.4$; plunging motion: $\theta_{\text{eff}} = 0.26 + 3.10 \sin(0.125\tau)$ deg, $M_\infty = 0.4$.

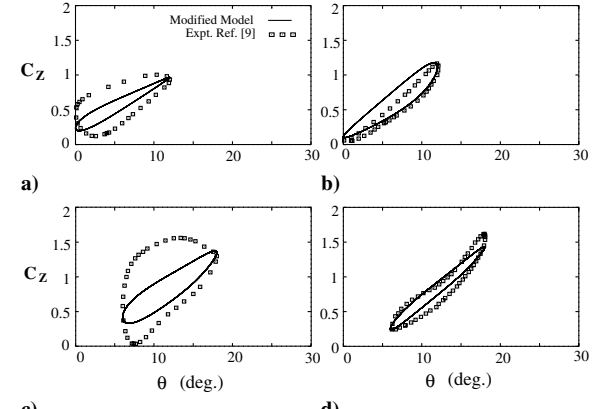


Fig. 5 Lift coefficient generated for pitching motion [$\theta = \theta_0 + 6 \cos(0.314\tau + \Phi)$ deg] in pulsating flow [$V = 6 + 2.136 \cos(0.314\tau)$ m/s]: a) $\theta_0 = 6$ deg, $\Phi = 0$ deg; b) $\theta_0 = 6$ deg, $\Phi = 180$ deg; c) $\theta_0 = 12$ deg, $\Phi = 0$ deg; d) $\theta_0 = 12$ deg, $\Phi = 180$ deg.

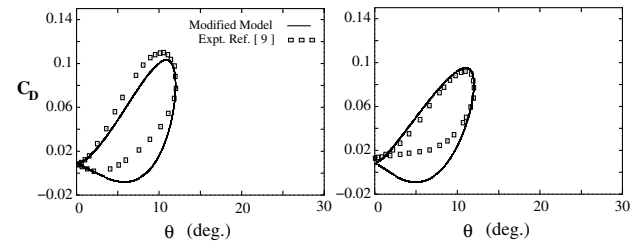


Fig. 6 Drag coefficient generated for a) pitching motion [$\theta = \theta_0 + 6 \cos(0.314\tau + \Phi)$ deg] and b) pitching motion in pulsating oncoming flow [$V = 6 + 2.136 \cos(0.314\tau)$ m/s], with $\Phi = 0$ deg.

6b respectively. The theoretical results show a very good correlation with experimental data.

4. Combined Pitching and Plunging Motion in Pulsating Oncoming Flow

For the purpose of illustration, theoretical data are generated for an airfoil (NACA 0012) undergoing combined pitching and plunging motion in time-varying oncoming flow, simulating the condition of a helicopter rotor blade cross section in operation. The data used for these calculations are

$$\begin{aligned} \theta &= \theta_0 + \theta_1 \cos(\omega t + \Phi); & \bar{h} &= \bar{h} \sin(\omega t) \\ V &= V_0 + \tilde{V} \cos(\omega t); & \bar{h} &= 0.42 \text{ m}; & V_0 &= 100 \text{ m/s} \\ \tilde{V} &= 39.6 \text{ m/s}; & b &= 0.2 \text{ m}; & \omega &= 25 \text{ rad/s}; & k &= 0.05 \\ \Phi &= 0 \text{ deg}; & \text{Case}(i) \theta_0 &= 6 \text{ deg} \\ \theta_1 &= 6 \text{ deg}; & \text{and Case}(ii) \theta_0 &= 12 \text{ deg}, & \theta_1 &= 6 \text{ deg} \end{aligned}$$

The results are generated for two pitch angle variations, one pertaining to low mean angle $\theta_0 = 6$ deg, and the other corresponding to high mean angle $\theta_0 = 12$ deg. The variation of aerodynamic coefficients are shown in Figs. 7a and 7b. Because there are no experimental data available for comparison, these results are presented for the sake of completeness and illustration.

B. 2-D Airfoil Response

The response of a 2-D airfoil undergoing pitching and plunging motion in a pulsating flow, simulating the condition of a typical cross section of a helicopter rotor blade in forward flight, is analyzed. Figure 8 shows a model of a 2-D airfoil undergoing pitching and plunging motions. The coupled equations of motion can be written as

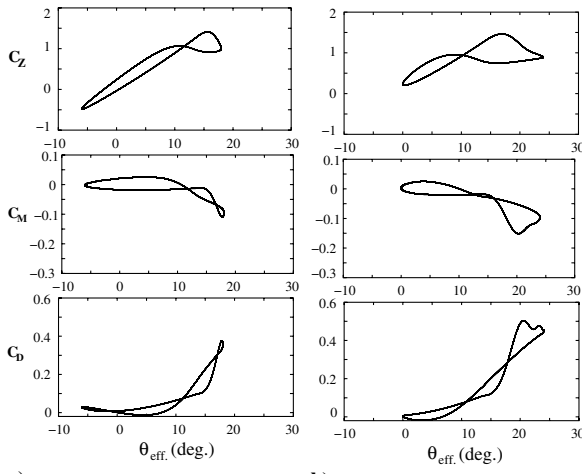


Fig. 7 Aerodynamic hysteresis loops for combined pitching and plunging motion ($\theta_{\text{eff}} = \theta + \dot{h}/V$ in degrees) in pulsating flow: a) $\theta_0 = 6$ deg, $\Phi = 0$ deg; b) $\theta_0 = 12$ deg, $\Phi = 0$ deg.

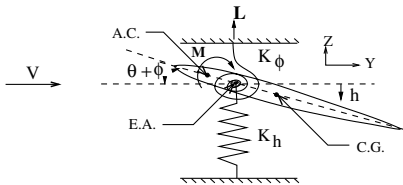


Fig. 8 2-D airfoil model.

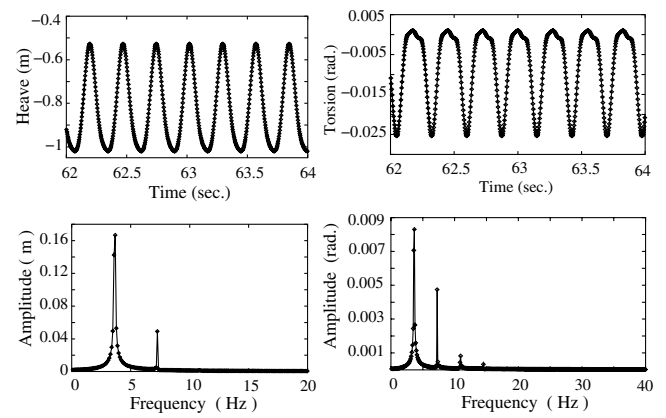
$$m\ddot{h} + S_\phi\ddot{\phi} + K_h h = -L \quad I_\phi\ddot{\phi} + S_\phi\ddot{h} + K_\phi\phi = M \quad (24)$$

where S_ϕ represents the inertia coupling.

The response of the airfoil is analyzed for different cases to bring out 1) the effect of dynamic stall modeling in comparison to quasi-steady approximation of Greenberg's aerodynamic theory [i.e., $C(k) \simeq 1$], and 2) influence of aeroelastic coupling (pitch-heave coupling due to S_ϕ) in association with dynamic stall. In evaluating the response of the airfoil, fourth-order Runge-Kutta integration scheme with a time step $\Delta t = 0.00314$ s, has been used. The instantaneous moment and lift acting on the airfoil are evaluated using Eqs. (4), (5), and (16–18), respectively. The response of the airfoil is calculated iteratively until steady state solution is arrived. The frequency contents of the response are obtained using Fast Fourier Transform (FFT). The data used in the calculations are $m = 7.95$ kg, $I_\phi = 0.115$ kg · m², $K_h = 4396.0$ N/m, $K_\phi = 734.2$ N · m, and $b = 0.209$ m. The input excitation frequency is $\Omega = 22.82$ rad/s (3.64 Hz). Input pitch angle θ and oncoming flow velocity are taken, respectively, as $\theta = 12 - 6 \cos(\Omega t)$ deg and $V = 113[1 + 0.40 \cos(\Omega t)]$ m/s. The uncoupled natural frequencies of the system are $\omega_h = 3.74$ Hz; $\omega_\phi = 12.72$ Hz.

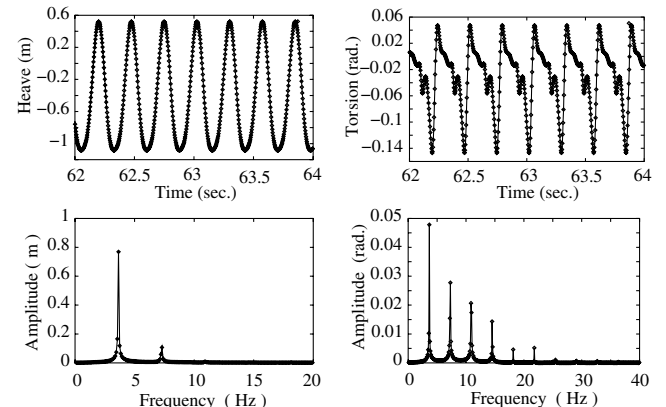
1. Uncoupled Response

In the uncoupled analysis, the aerodynamic center (A.C.), center of mass (C.G.), and elastic axis (E.A.) are assumed to be located at the quarter-chord point of the 2-D airfoil. The response of the airfoil is obtained using two aerodynamic models, namely, quasi-steady aerodynamic model and modified stall model. Heave and torsional responses for quasi-steady aerodynamic theory and their frequency contents are plotted in Figs. 9a and 9b, respectively. The response for modified stall model and their frequency contents are plotted in Figs. 10a and 10b, respectively. The heave response obtained from the quasi-steady aerodynamic theory contains two frequencies, namely, 3.64 Hz and 7.27 Hz, whereas torsional response contains three frequencies (3.64 Hz, 7.27 Hz, and 10.90 Hz), which are integer multiples of excitation frequency 3.64 Hz. Table 1 shows the frequency contents and their magnitude of the uncoupled heave



a) Heave

Fig. 9 Uncoupled airfoil response for quasi-steady aerodynamic theory.



a) Heave

Fig. 10 Uncoupled airfoil response for modified stall model.

response for quasi-steady and modified stall aerodynamic theory. It is observed that the amplitude of the heave response for the case of modified stall model is three times greater than that for the quasi-steady model. In the case of torsional mode, modified stall model introduces additional harmonics (Table 2), as compared to quasi-steady aerodynamics. The reason for the appearance of additional higher harmonics may be attributed to the nonlinearity of the stall model.

Table 1 Uncoupled heave response for quasi-steady and modified stall aerodynamic theory

	Quasi-steady	Dynamic stall
Frequency, Hz	Magnitude, m	Magnitude, m
3.64	0.23	0.77
7.27	0.05	0.11

Table 2 Uncoupled torsional response for quasi-steady and modified stall aerodynamic theory

	Quasi-steady	Dynamic stall
Frequency, Hz	Magnitude, rad	Magnitude, rad
3.64	0.008	0.048
7.27	0.005	0.028
10.90	0.001	0.021
14.53	—	0.014
18.20	—	0.005

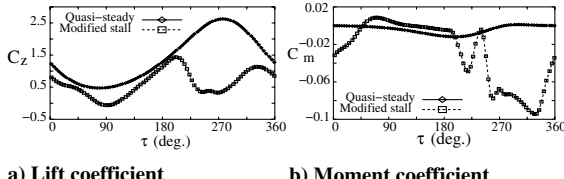


Fig. 11 Comparison of quasi-steady lift and moment with modified stall model lift and moment.

Lift and moment obtained from quasi-steady aerodynamics and modified stall model are plotted for one cycle in Figs. 11a and 11b, respectively. The variation of lift coefficient shows that the minimum occurs at 77 deg for quasi-steady aerodynamic theory, and for modified stall model it is shifted to 95 deg. The peak value of the lift coefficient for dynamic stall is lower than that corresponding to quasi-steady aerodynamics. The stall model also introduces additional harmonics in lift and moment coefficients.

2. Coupled Response

In the coupled analysis, heave-pitch coupling is introduced by shifting the mass center from the elastic axis. Elastic axis and aerodynamic center are located at quarter-chord point. The influence of aeroelastic coupling on the airfoil response has been studied for various values of S_ϕ by shifting the mass center aft and forward of elastic axis. For the sake of conciseness, only few cases are discussed in the following.

Figures 12–17 show the response and frequency contents along with phase plane diagram for the heaving and pitching motion of the airfoil for various aft locations of center of mass from elastic axis, namely, 3, 4, and 5% of the chord. A comparison of these figures shows that as the pitch-heave coupling is increased (i.e., by shifting the center of mass aft of elastic axis), pitch and heave motions of airfoil become qualitatively different. Increasing the coupling seems to increase the distribution of frequency contents in the response signal, as observed in Figs. 12, 14, and 16. The phase plane diagrams (Figs. 13, 15, and 17) show that as the coupling is increased, the motion of the airfoil changes from periodic to bounded chaotic motion.

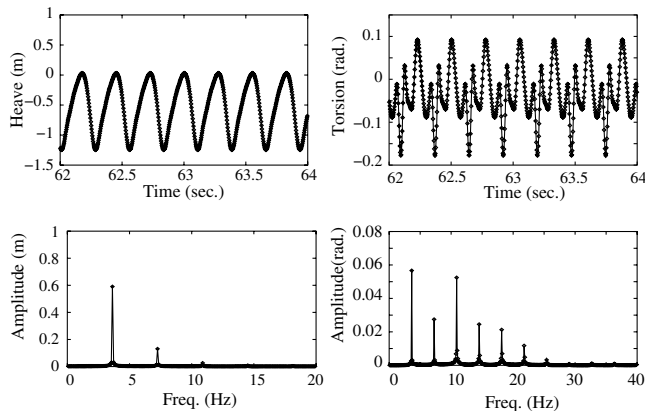


Fig. 12 Airfoil response and its frequency contents generated with modified stall model for 3% chord aft location of C.G. from E.A.

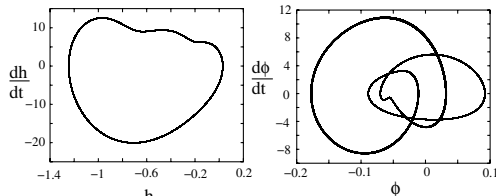


Fig. 13 Phase plane diagrams of airfoil response generated with modified stall model for 3% chord aft location of C.G. from E.A.

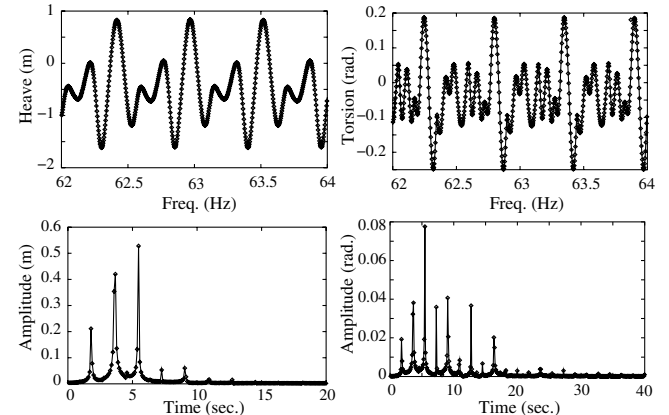


Fig. 14 Airfoil response and its frequency contents generated with modified stall model for 4% chord aft location of C.G. from E.A.

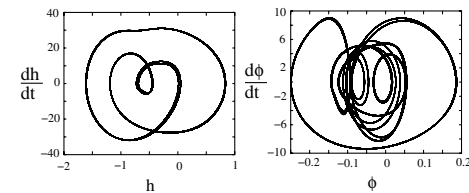


Fig. 15 Phase plane diagrams of airfoil response generated with modified stall model for 4% chord aft location of C.G. from E.A.

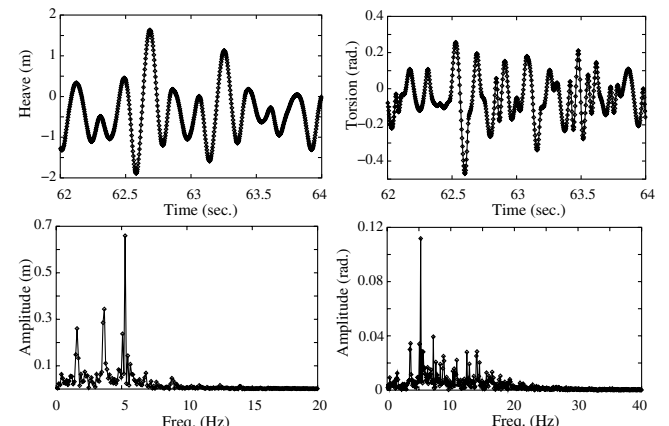


Fig. 16 Airfoil response and its frequency contents generated with modified stall model for 5% chord aft location of C.G. from E.A.

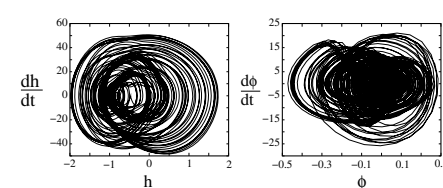


Fig. 17 Phase plane diagrams of airfoil response generated with modified stall model for 5% chord aft location of C.G. from E.A.

Table 3 shows the frequency distribution of the response and the magnitude, for different cases of center of mass location from elastic axis of the airfoil. It can be seen that the uncoupled (0% chord) and the coupled (3% chord aft location of center of mass from elastic axis) have same frequency contents but different magnitudes. The frequencies correspond to the excitation frequency of the input 3.64 Hz and its higher harmonics. When the center of mass location is shifted to 4% chord aft of the elastic axis, the airfoil response shows significant subharmonic (1.82 Hz which is half of input frequency 3.64 Hz) and superharmonic frequency contents. For the case of 5%

Table 3 Frequency distribution of airfoil response with modified stall model and aeroelastic coupling

Frequency (Hz)	Magnitude of heave response, m					Magnitude of torsional response, rad				
	Aft location of C.G. from E.A.					Aft location of C.G. from E.A.				
	0%	3%	4%	5%	0%	3%	4%	5%		
0.40	—	—	—	0.063	—	—	—	—	0.009	
1.59	—	—	—	0.260	—	—	—	—	0.013	
1.82	—	—	0.213	0.016	—	—	—	0.019	0.002	
1.89	—	—	—	0.063	—	—	—	—	0.003	
2.18	—	—	—	0.074	—	—	—	—	0.003	
3.08	—	—	—	0.064	—	—	—	—	0.003	
3.64 ^a	0.768	0.592	0.422	0.344	0.048	0.057	0.038	0.034		
4.77	—	—	—	0.084	—	—	—	—	0.009	
5.07	—	—	—	0.237	—	—	—	—	0.034	
5.27	—	—	—	0.659	—	—	—	—	0.112	
5.45	—	—	0.533	0.143	—	—	—	0.078	0.029	
5.66	—	—	—	0.106	—	—	—	—	0.028	
6.36	—	—	—	0.041	—	—	—	—	0.017	
7.27 ^a	0.113	0.132	0.048	0.033	0.028	0.027	0.036	0.039		
7.66	—	—	—	0.030	—	—	—	—	0.021	
8.95	—	—	—	0.036	—	—	—	—	0.021	
9.10	—	—	0.058	0.023	—	—	—	0.041	0.008	
10.54	—	—	—	0.008	—	—	—	—	0.016	
10.90 ^a	0.008	0.025	0.017	0.015	0.021	0.052	0.008	0.022		
12.53	—	—	—	0.015	—	—	—	—	0.028	
12.72	—	—	0.015	0.007	—	—	—	0.036	0.008	
14.12	—	—	—	0.011	—	—	—	—	0.031	
14.53 ^a	—	0.008	0.006	0.003	0.014	0.024	0.007	0.020	0.020	
16.35	—	—	0.004	0.002	—	—	—	0.020	0.013	
18.20 ^a	—	—	0.004	0.003	0.005	0.022	0.003	0.005		
19.98	—	—	—	0.002	—	—	—	0.003	0.002	

^aIndicates excitation frequency of the input (3.64 Hz) and its higher harmonics.

chord aft location of center of mass from elastic axis, the response contains several frequencies which are noninteger multiple of excitation frequency, both below and above the excitation frequency. The magnitudes of these additional frequency contents are comparable to the magnitudes of the response at input excitation frequency.

To verify whether the motion is truly chaotic or not, computations were performed to study the effect of perturbation in initial condition on the steady state response of the system. If the steady state response is sensitive to perturbation in initial conditions, it represents chaotic motion [34] and the Liaponov exponent provides a quantitative measure of the chaotic motion. The response of the airfoil is evaluated for two different sets of initial conditions, namely, 1) all initial conditions are zero, and 2) perturbed initial condition with $\phi(0) = 0.01$ and other initial conditions are set to zero. The magnitude of the difference in the response of the airfoil in pitch ($|\phi_2 - \phi_1|$) and heave ($|h_2 - h_1|$) is plotted as function of time. (Note: Subscript 1 represents the response corresponding to all zero initial conditions, whereas subscript 2 represents the case corresponding to perturbed initial condition.) If the steady state response is independent of the perturbation in initial conditions (i.e., $|\phi_2 - \phi_1|_{t \rightarrow \infty} = 0$, $|h_2 - h_1|_{t \rightarrow \infty} = 0$), then it indicates periodic response. On the other hand, if the response is sensitive to perturbations in initial conditions, it represents chaotic motion [34]. Figure 18 shows the sensitivity of the response to initial conditions for three cases of center of mass locations. It is evident that the system is insensitive to initial condition for the two cases of center of mass location, namely, at 0 and 3% chord aft of elastic axis, as shown in Figs. 18a and 18b, respectively. For the case of center of mass location at 5% chord aft of elastic axis, the response of the system is sensitive to the perturbation in initial condition as shown in Fig. 18c. The Liaponov exponent is obtained from the plots of $\ln |(\phi_2 - \phi_1)/\delta|$ and $\ln |(h_2 - h_1)/\delta|$ vs time, where δ is the perturbation in initial condition. The positive slope of the mean curve is defined as Liaponov exponent and it represents the sensitivity of the response to perturbation in initial conditions. If the mean slope reaches a steady value, it indicates a bounded chaotic motion. From Fig. 19, it can be

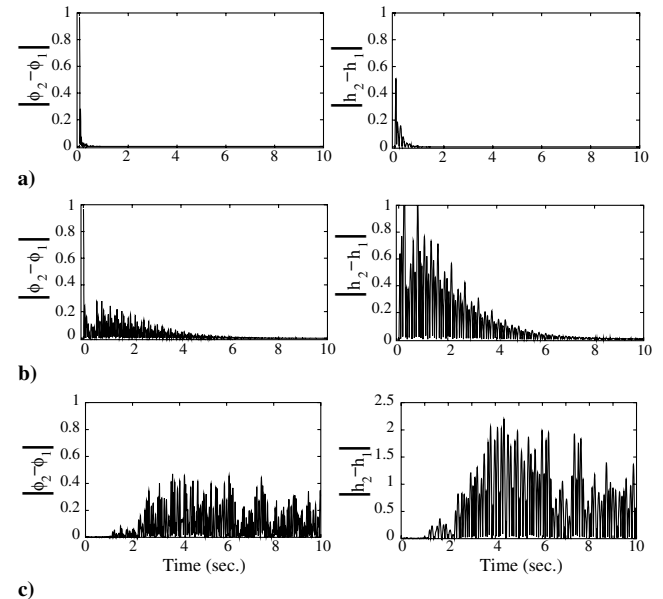


Fig. 18 Magnitude of the difference in response for two different initial conditions as a function of time for a) 0%, b) 3%, and c) 5% chord aft location of C.G. from E.A.

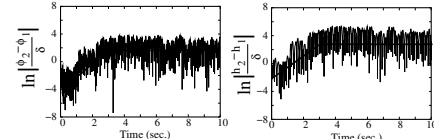


Fig. 19 Liaponov exponents (slope of the mean curve, solid line) for pitch and heave motion for 5% chord aft location of C.G. from E.A.

seen that both pitch and heave motion indicate bounded chaotic motion, with Liapponov exponents 1.78 for pitch and 1.48 for heave.

These results show that dynamic stall (nonlinear aerodynamics) in association with aeroelastic pitch-heave coupling above a certain level can lead to bounded chaotic motion of the airfoil.

Further rearward shift of mass center (about 7% of the chord), leads the system to become completely unstable. However, forward shift of mass center always gives rise to a stable periodic response similar to the uncoupled case. Additional results pertaining to different locations of mass center can be found in [35].

IV. Conclusions

ONERA(EDLin) dynamic stall model has been analyzed in relation to Theodorsen's and Greenberg's unsteady aerodynamic theories. It is shown that ONERA(EDLin) dynamic stall model in the unstalled region is identical to Theodorsen's model, except that lift deficiency function $C(k)$ is approximated by a first-order rational approximation. Replacing the first-order rational approximation by a more accurate second-order rational approximation, a modified dynamic stall model is proposed in this study. This improved stall model is shown to provide a better correlation with experimental stall data.

Using the modified stall model, the response characteristics of a 2-D airfoil undergoing pitching and plunging motion in a pulsating oncoming flow are analyzed to study the effects of dynamic stall. The results of this study show that significant difference is observed in the response of airfoil for dynamic stall and quasi-steady aerodynamic models. The results of this study also show that dynamic stall in association with aeroelastic couplings above a certain level leads to bounded chaotic motion of the airfoil.

Appendix: Aerodynamic Characteristics of Airfoil

I. Symmetrical Airfoil [17]

Static lift data:

$$C_{z_l} = p_0 \theta; \quad p_0 = 0.10(1 - M_\infty^8) / \sqrt{1 - M_\infty^2} \quad (A1)$$

$$\Delta C_z = \begin{cases} 0 & \theta < \theta_d \\ (p_0 - p_1)(\theta - \theta_d) - c_1 \{ \exp[h_1(\theta - \theta_d)] - 1 \} & \theta \geq \theta_d \end{cases} \quad (A2)$$

where

$$\begin{aligned} \theta_d &= 15(1 - M_\infty^2) & p_1 &= 0.1M_\infty^4 & c_1 &= 0.7(1 - M_\infty) \\ h_1 &= -0.5 + (1.5 - M_\infty)M_\infty^2 \end{aligned}$$

Static moment data:

$$C_{m_l} = 0.0 \quad (A3)$$

$$\Delta C_m = \begin{cases} 0 & \theta < \theta_d \\ c_2 \{ \exp[h_2(\theta - \theta_d)] - 1 \} & \theta \geq \theta_d \end{cases} \quad (A4)$$

where

$$\begin{aligned} c_2 &= -0.09 - 0.08 \exp[-30(M_\infty - 0.6)^2] \\ h_2 &= -0.4 - 0.21 \tan^{-1}[22(0.45 - M_\infty)] \end{aligned}$$

Static drag data:

$$C_{d_0} = 0.008 \quad (A5)$$

$$\Delta C_d = \begin{cases} 0 & \theta < \theta_d \\ (C_{d_0} - 0.30)[1 - [(\theta_{\max} - \theta) / (\theta_{\max} - \theta_d)]^u] & \theta \geq \theta_d \end{cases} \quad (A6)$$

where

$$\begin{aligned} \theta_{\max} &= 25 & \theta_{\text{Mach}} &= 18 - 2 \tan^{-1}(4M_\infty) \\ u &= (\theta_{\max} - \theta_d) / (\theta_{\text{Mach}} - \theta_d) \end{aligned}$$

II. Unsymmetrical Airfoil [13]

Static lift data:

$$C_{z_l} = 0.11831 \theta_{\text{eff}} \quad (A7)$$

Static moment data:

$$C_{m_l} = 0.001666 \theta_{\text{eff}} \quad (A8)$$

References

- [1] Friedmann, P. P., and Hodges, D. H., "Rotary Wing Aeroelasticity—A Historical Perspective," *Journal of Aircraft*, Vol. 40, No. 6, 2003, pp. 1019–1046.
- [2] Bousman, W. G., "Putting the Aero Back into Aeroelasticity," *Proceedings of the 8th ARO Workshop on Aeroelasticity of Rotorcraft Systems*, Pennsylvania State University, University Park, PA, 1999.
- [3] Lytwyn, R. T., "An Analysis of the Divergent Vertical Helicopter Oscillations Resulting from the Physical Presence of the Pilot in the Collective Control Loop," *Proceedings of the 22nd Annual Forum of the American Helicopter Society*, American Helicopter Society, Alexandria, VA, 1966, pp. 45–52.
- [4] Dowell, E. H., and Ilgamav, M., *Studies in Nonlinear Aeroelasticity*, Springer-Verlag, New York, 1988, pp. 1–3.
- [5] McCroskey, W. J., Carr, L. W., and McAlister, K. W., "Dynamic Stall Experiments on Oscillating Airfoils," *Journal of Aircraft*, Vol. 14, No. 1, Jan. 1976, pp. 57–63.
- [6] McCroskey, W. J., McAlister, K. W., Carr, L. W., and Pucci, S. L., "An Experimental Study of Dynamic Stall on Advanced Airfoil Sections," Vol. 1, "Summary of the Experiment"; Vol. 2, "Pressure and Force Data"; Vol. 3, "Hot-Wire and Hot-Film Measurements," NASA TM-84245, 1982.
- [7] Carta, F. O., "A Comparison of Pitching and Plunging Response of an Oscillating Airfoil," NASA CR-3172, Oct. 1979.
- [8] Ericsson, L. E., and Reding, J. P., "The Difference Between the Effects of Pitch and Plunge on Dynamic Airfoil Stall," *Proceedings of the 9th European Rotorcraft Forum*, Stresa, Italy, 1983, pp. 8.1–8.8.
- [9] Favier, D., Agnes, A., Barbi, C., and Maresca, C., "Combined Translation/Pitch Motion: A New Airfoil Dynamic Stall Simulation," *Journal of Aircraft*, Vol. 25, No. 9, 1988, pp. 805–814.
- [10] Beddoes, T. S., "A Synthesis of Unsteady Aerodynamic Effects Including Stall Hysteresis," *Vertica*, Vol. 1, No. 2, 1976, pp. 113–123.
- [11] Gangwani, S. T., "Prediction of Dynamic Stall and Unsteady Airloads for Rotor Blades," *Proceedings of the 37th Annual Forum of the American Helicopter Society*, American Helicopter Society, Alexandria, VA, 1981, pp. 1–17.
- [12] Leishman, J. G., and Beddoes, T. S., "A Generalized Model for Airfoil Unsteady Aerodynamic Behavior and Dynamic Stall Using the Indicial Method," *Proceedings of the 42nd Annual Forum of the American Helicopter Society*, American Helicopter Society, Alexandria, VA, 1986, pp. 243–265.
- [13] Tyler, J. C., and Leishman, J. G., "Analysis of Pitch and Plunge Effects on Unsteady Airfoil Behavior," *Journal of the American Helicopter Society*, Vol. 37, No. 3, July 1992, pp. 69–82.
- [14] Van der Wall, B. G., and Leishman, J. G., "On the Influence of Time-Varying Flow Velocity on Unsteady Aerodynamics," *Journal of the American Helicopter Society*, Vol. 39, No. 4, Oct. 1994, pp. 25–36.
- [15] Petot, D., "Progress in the Semi-Empirical Prediction of the Aerodynamic Forces due to Large Amplitude Oscillations of an Airfoil in Attached or Detached Flow," ONERA TP 1983-111, 1983, pp. 1–22.
- [16] Peters, D., "Toward a Unified Lift Model for Use in Rotor Blade Stability Analysis," *Journal of the American Helicopter Society*, Vol. 30, No. 3, July 1985, pp. 32–42.
- [17] Petot, D., "Differential Equation Modeling of Dynamic Stall," La Recherche Aérospatiale, Paper No. 1989-5, 1989.
- [18] Truong, V. K., "Prediction of Helicopter Rotor Airloads Based on Physical Modeling of 3-D Unsteady Aerodynamics," *Proceedings of the 22nd European Rotorcraft Forum*, Brighton, U.K., 1996, pp. 96.1–96.14.

- [19] Tan, C. M., and Carr, L. W., "The AFDD International Dynamic Stall Workshop on Correlation of Dynamic Stall Models with 3-D Dynamic Stall Data," NASA TM-110375, 1996.
- [20] Srinivasan, G. R., Ekaterinaris, J. A., and McCroskey, W. J., "Evaluation of Turbulence Models for Unsteady Flows of an Oscillating Airfoil," *Computers & Fluids*, Vol. 24, No. 7, Sept. 1995, pp. 833–861.
- [21] Ekaterinaris, J. A., and Platzer, M. F., "Computational Prediction of Airfoil Dynamic Stall," *Progress in Aerospace Sciences*, Vol. 33, Nos. 11–12, April 1998, pp. 759–846.
- [22] Chanduru, S. J., Subramanian, S., and Goankar, G. H., "Dynamic Stall and Wake Effects on Trim and Stability of Hingeless-Rotor with Experimental Correlation," *Journal of the American Helicopter Society*, Vol. 42, No. 3, Oct. 1997, pp. 370–382.
- [23] Tang, D., and Dowell, E. H., "Nonlinear Rotor Aeroelastic Analysis with Stall and Advanced Wake Dynamics," *Journal of Aircraft*, Vol. 34, No. 5, Sept. 1997, pp. 679–687.
- [24] Meyer, M., and Matthies, H. G., "State-Space Representation of Instationary Two-Dimensional Airfoil Aerodynamics," *Journal of Wind Engineering and Industrial Aerodynamics*, Vol. 92, Nos. 3–4, 2004, pp. 263–274.
- [25] Petot, D., Arnaud, G., Harrison, R., Stevens, J., Dieterich, O., Van der Wall, B. G., Young, C., and Széchenyi, E., "Stall Effects and Blade Torsion—An Evaluation of Predictive Tools," *Journal of the American Helicopter Society*, Vol. 44, No. 4, Oct. 1999, pp. 320–331.
- [26] Larsen, J. W., "Nonlinear Dynamics of Wind Turbine Wings," Ph.D. Thesis, Dept. of Civil Engineering, Aalborg Univ., Denmark, July 2005.
- [27] Laxman, V., and Venkatesan, C., "Dynamic Stall Modeling and Its Effect on Airfoil Response," *Proceedings of the 11th International Workshop on Rotorcraft Dynamics and Aeroelasticity*, Florida Atlantic University, Boca Raton, FL, Oct. 2005.
- [28] Depailler, G., and Friedmann, P. P., "Reductions of Vibrations due to Dynamic Stall in Helicopters Using an Actively Controlled Flap," AIAA Paper 2002-1431, April 2002.
- [29] Tang, D., and Dowell, E. H., "Chaotic Stall Response of a Helicopter Rotor in Forward Flight," *Journal of Fluids and Structures*, Vol. 6, No. 3, 1992, pp. 311–336.
- [30] Tang, D., and Dowell, E. H., "Comparison of Theory and Experiment for Non-Linear Flutter and Stall Response of a Helicopter Blade," *Journal of Sound and Vibration*, Vol. 165, No. 2, 1993, pp. 251–276.
- [31] Theodorsen, T., "General Theory of Aerodynamic Instability and the Mechanism of Flutter," NACA Technical Report 496, 1935.
- [32] Venkatesan, C., and Friedmann, P. P., "A New Approach to Finite State Modelling of Unsteady Aerodynamics," *AIAA Journal*, Vol. 24, No. 12, 1986, pp. 1889–1897.
- [33] Greenberg, M. J., "Airfoil in Sinusoidal Motion in a Pulsating Stream," NASA Technical Report 1326, 1947.
- [34] Strogatz, S. H., *Nonlinear Dynamics and Chaos*, Westview, New York, 1994, pp. 317–367.
- [35] Laxman, V., and Venkatesan, C., "Dynamic Stall and Dynamic Wake Models for Helicopter Aeroelastic Applications," Technical Report, Department of Aerospace Engineering, IIT Kanpur, India, 2005.

E. Livne
Associate Editor